Diverse Lunar Polar Permanently Shadowed Regions and Environmental Metrics for Site Planning Decision-Making

C. J. Ahrens[1,2], J. Fastook[3], and N.E. Petro[2]

[1]CRESST-II, University of Maryland, College Park, Maryland, USA.
8800 Greenbelt Rd., B34/Caitlin Ahrens, Greenbelt, MD 20771
Caitlin.ahrens@nasa.gov

[2]NASA Goddard Space Flight Center, Greenbelt, Maryland, USA.
8800 Greenbelt Rd., B34/Noah Petro, Greenbelt, MD 20771
Noah.e.petro@nasa.gov

[3]University of Maine, Climate Change Institute, Orono, Maine, USA.
University of Maine, Orono, ME 04469
fastook@maine.edu

Corresponding author: Caitlin Ahrens (Caitlin.ahrens@nasa.gov)

Abstract

The key element in the characterization and operational planning of volatile behavior at the lunar poles is to assess the environmental variability of Permanently Shadowed Regions (PSRs) at the lunar poles. These PSRs can be classified into three main types (A, B, and C) based on their physical distribution within the host crater (due to topography and illumination environmental characteristics). We find that the surficial emplacement of these volatiles may also be linked to subsurface thermal variability, which influences volatile retention. Understanding the environmental factors allows for the comparison of PSRs for the context of scientific objectives, like for Artemis, and for the development of effective and adaptive decision-making capabilities for site and resource operation planning. This paper discusses the diverse nature of PSRs for scientific objective and site planning perspectives, including environmental metrics that decision-making frameworks can utilize.

Keywords: Lunar resources; Mapping; Lunar volatiles; Decision-Making; Site Planning

1 Introduction

The permanently shadowed regions (PSRs) at the lunar poles have been characterized by the variations in seasonal temperatures (resultant from the low obliquity 1.54° angle between the Moon's pole spin and the ecliptic plane; Siegler et al. 2011) by the Diviner Lunar Radiometer Experiment onboard the Lunar Reconnaissance Orbiter (Tooley et al. 2010; Kloos et al. 2019; Wilcoski et al. 2023), along with topographic relief and lack of an atmosphere (Margot 1999; Mazarico et al. 2011; Hodges 2018; Landis et al. 2022). Since the illumination in the polar regions are perpetually at grazing angles, topography must play a major role in surface temperatures (Bussey et al. 1999, 2010; McGovern et al. 2013; Gläser et al. 2018; Williams et al. 2019). With surface temperatures within craters < 110 K, these are capable of cold trapping water over ~1 Gyr, and some areas even maintain temperature conditions < 30 K (Paige et al. 2010; Colaprete et al. 2010; Hayne et al. 2015; Li et al. 2018). Such thermal environment variations (e.g., time, season) can make studying these PSRs complex. For example, Durga Prasad et al. (2022) presented a 3D finite element model using DEMs and Apollo 17 data designed to simulate the thermophysical behavior of the lunar surface and subsurface in modulating heat transfer, aligning with prior findings that such structure influences thermal insulation and energy storage within the regolith. This thermophysical behavior is critical to volatile transport dynamics, as temperature gradients and thermal conductivity affect sublimation, migration, and re-deposition of volatiles like water ice. Due to this temperature variability, there may be variations in chemical species condensed at the PSRs (namely due to different chemicals having various condensation and sublimation conditions; Hurley et al. 2023), such as water ice and volatile species like carbon dioxide or sulfur dioxide, as observed by Chandrayaan-1's Moon Mineralogy Mapper (M^3) and other missions (Sanin et al. 2012; Fisher et al. 2017; Li et al. 2018; Schörghofer et al. 2021a,b). The origin of these volatile species may be a combination of internal sources (volcanic and volatile outgassing; Kring et al. 2021) and external sources (cometary or solar wind interactions; McCord et al. 2011; Schörghofer et al. 2021a).

PSRs have been defined by being regions of permanent shadow, but not in an organized survey based on the physical distribution (herein defined as emplacement) within the host crater of potentially varying volatile chemistry and thermal properties of the regolith. PSR orientations

within their respective host craters or depressions, temperature variations, and crater slopes would not hold true for all PSRs. Prior studies of PSRs have identified PSRs solely by size (i.e., micro-PSRs by Hayne et al. 2021) or simply distribution of potential frozen materials across the lunar poles (Brown et al. 2022; Schörghofer & Rufu 2023; Bickel et al. 2022). Several studies and white papers for Artemis sample collection and curation have begun to strategize and invest in determining sample variations during surface collection at the lunar south pole and highlighting the need for varied settings, including varying thermal environments and collection sites within and proximal to PSRs (Mitchell et al. 2020; Gross et al. 2022; Noble et al. 2024).

Site planning is essential to plan all factors of operations, from environmental and economic sustainability, resource management, and geostrategic systems with international entities. Such planning involves making explicit decisions on a spatial scale about the types of resources and land uses allowable, and the location and extent for operations (Bryan 2003). Surveying the PSR sites pre-landing gives an opportunity to plan for environmental factors into resource management, mining operations, PSR conservation, and other lunar surface activities. The spatial and environmental variability of these PSRs must be necessary for decision-making frameworks to support science, engineering, and management activities and decisions. However, environmental uncertainties (e.g., abundances of ice at PSRs, locality of PSRs during certain seasons, resourcefulness versus hazards at PSRs) can lead to variations in decision-making efforts, leading to the need for adaptable support frameworks. Surveying these PSRs ahead of time can reduce cost and time, though such operational decisions will improve with further ground-truthing at PSRs. A spatial survey on the diversity of these PSR areas at the lunar poles can also assist in knowing the multitude of parameters affecting the land use distribution, including both natural and human parameters that can influence the distribution and accumulation of volatiles at the poles in short- and long-term presence on the Moon. Beginning metrics to evaluate multiple (and variable) sites are crucial for effective scientific landscape analyses, resource management decision-making frameworks, and the future establishment of environmental databases and models of the lunar poles.

We believe that surveying PSRs into distinctive, yet basic, types based on their morphological parameters (size, slope, temperature, etc.) is a more productive method for both understanding their physical processes and organizing for surveying (and in-situ resource utilization ISRU planning) purposes. Here we describe the environmental factors that influence PSR variability, and how these factors can be useful for surface operation and resource management decision-making frameworks.

2 Methods

On Earth, topography is a major factor on the spatial distribution of physical environmental parameters, from soil chemistry, solar radiation, and temperature (Bryan 2003). These factors are also related to the diversity of PSRs at the lunar poles. We have analyzed a sample size of 68 PSRs (> 10 km^2 area) at the lunar poles (33 and 35 at the north and south poles, respectively). Note that we did not analyze non-crater PSRs or micro-PSRs as we wanted to evaluate macro-scale thermally various areas for PSR emplacement (Hayne et al. 2021; Thomson et al. 2023). We used the Lunar Reconnaissance Orbiter Camera (LROC) QuickMap and JMARS (Java Mission-planning and Analysis for Remote Sensing; v5.3.14) programs to upload and analyze data from LRO, using the Diviner (bolometric temperature at ~250 m/px resolution; Williams et al. 2019), LROC imagery (0.5 m/px; Robinson et al. 2010), and LOLA

(slopes and illumination; Mazarico et al. 2011) instruments. In addition, we have also obtained deconvolved Lunar Prospector hydrogen maps in QuickMap (Wilson et al. 2018). LROC QuickMap also has a digitization map of PSRs of > 1 km^2 from Mazarico et al. (2011) using LOLA topography (~60 m/px from 82 – 90°S; ~120 m/px from 75 – 82°S). Crater slope topography (of which PSRs are also observed) have been analyzed using LOLA (Gläser et al. 2014) by measuring the elevation difference of the crater rim (specifically where the PSR is seasonally dominant) and crater floor and cross-referenced with crater wall slopes measured from Landis et al. (2022). From the Diviner temperatures, we used the maximum summer and winter seasons, as mapped from Williams et al. (2019) in the LROC QuickMap program, to measure temperature differences of the PSRs with their host crater environments.

To determine the maximum volatile ice emplacement within a crater, the University of Maine Ice Sheet Model (UMISM) was used, a finite element shallow-ice model that has been used on Earth (Hooke & Fastook 2007), Mars' frozen volatiles (Fastook et al. 2012; Fastook & Head 2015), and Mercury PSRs (Fastook et al. 2019). For this model, we assume regolith characteristics from previous lunar thermal models at the lunar south pole, some of which use Apollo-specific thermal estimates of the regolith (Horai and Fujii 1972; Liu et al. 2019). We also presume that the frozen volatiles at the PSRs are ice-rich, not fully intermixed with the regolith composition. While this end-member example greatly exceeds expectations of realistic volumes for ice-deposits at the Moon (< 1 m; Liu et al. 2019; Brown et al. 2022), therefore we model the maximum ice thickness potential in the crater.

Boundary conditions for the thermodynamic component includes (i) the mean-annual surface temperature (taken as 26 K for the shadowed regions and 389 K for the average sunlit areas; Paige et al. 2010; Hayne et al. 2017), and (ii) an upper bound basal geothermal heat flux as 10 mW m^{-2} based on the Apollo Heat Flow Experiment (Siegler & Smrekar 2014; Fastook et al. 2019). This model constrains the PSR ice filling volume to be the crater depth and shallow slope (i.e., the sun angle ~89°). Within the model, ice properties that control deposition (including downslope on crater walls) are functions of temperature, and accounts for indirect and geothermal heat flux (Fastook et al. 2019).

3 Results

3.1 PSR Survey

The components used to determine PSR "types" were the size and area of the PSR with respect to their host crater or depression, and slope of the PSR on the crater wall. The morphology of the PSR was determined by how the boundaries are mapped within the crater (in LROC QuickMap) as to whether the PSR boundary was entirely within the crater or cohesively on the crater wall, though some PSRs are partial and segmented on the crater wall. These boundaries are then used to measure PSR area with respect to the host crater area (PSR/Crater area ratio). The crater slope is then measured against the PSR/Crater ratio to distinguish between the PSR types and how slope is a defining parameter in this classification. PSRs and their respective type used in this study are shown in Table 1.

Table 1: Catalog of PSRs used in this study with location coordinates, measured area, and classification type.

Pole	PSR area	Latitude	Longitude	PSR Area (km^2)	Type
South	Shackleton	-89.695	126.371	318.62	A
	Malinkin	-87.228	76.216	53.28	A
	Haworth	-87.529	-4.854	1581.15	A
	Idel'son	-84.024	118.15	435.6	A
	Ibn Bajja	-86.22	-74.695	101.2	A
	Svedberg	-81.656	65.207	129.92	A
	von Baeyer	-81.718	61.383	109	A
	de Gerlache	-88.275	-90.629	355.34	B
	Faustini	-87.1331	84.499	710.64	B
	Slater	-88.1177	112.068	274.04	B
	Unnamed	-87.437	118.86	79.2	B
	Unnamed	-86.9617	107.096	134.55	B
	Amundsen	-83.695	90.443	2456.16	B
	Kuhn	-84.41	-151.993	75.69	B
	Wiechert J	-85.168	-177.513	318.4	B
	Wiechert E	-83.532	175.827	122	B
	Weichert U	-83.352	149.434	195.92	B
	Wiechert	-83.795	163.512	390.08	B
	SW-Malapert F	-82.208	11.23	307.8	B
	Shoemaker	-88.057	44.313	1221.3	B
	Cabeus B	-81.64	-54.49	587.06	B
	Sverdrup	-88.29	-148.585	229.62	B
	Unnamed	-88.704	169.562	21.6	B
	Unnamed	-88.337	147.092	32.39	B
	Nefed'ev	-80.4976	135.387	370.88	B
	Kocher	-84.387	-134.735	77	B
	Malapert	-84.167	6.41	327.6	B
	Scott E	-80.942	35.584	183.04	B
	Nobile	-85.363	51.569	178.48	C
	Cabeus 1	-84.445	-45.305	414.96	C
	Cabeus 2	-84.615	-36.483	72.8	C
	Wiechert P	-84.822	150.006	109.04	C
	Scott	-80.789	45.177	110.04	C
	Cabeus Floor 1	-85.3505	-42.07	71.25	C
	Cabeus Floor 2	-85.389	-51.804	81.4	C
North	Whipple	89.13	120.57	123.05	A
	Hinshelwood	89.34	307.515	83.16	A
	Hermite A	87.992	308.85	282.828	A
	Erlanger	86.992	28.96	86.955	A
	Plaskett U	82.42	162.366	138.99	A
	Gringnard	84.471	284.73	82.68	A
	Slyvester N	82.36	291.793	216.08	A
	Crater in Nansen	82.269	64.36	201.55	A
	Fibiger	86.117	37.016	130.56	B

Nansen D	83.62	65.66	107.8	B
Nansen E	83.243	72.339	33.92	B
Nansen F	84.348	62.05	422.82	B
Houssay	82.925	98.668	190	B
Unnamed	84.288	97.99	65.52	B
Unnamed	84.747	93.48	66.5	B
Bosch	86.697	131.712	61.42	B
RozhdestvenskiyU	84.497	153.445	386.65	B
RozhdestvenskiyK	81.868	213.27	438.11	B
RozhdestvenskiyH	82.99	227.04	61.56	B
Lovelace	81.464	250.166	382.2	B
Unnamed	83.274	304.64	27.65	B
Plaskett V	81.582	121.39	254.04	B
Nansen	82.477	66.867	26.24	C
RozhdestvenskiyW	84.86	113.64	113	C
Hevesy	82.476	150.36	92.34	C
Rozhdestvenskiy	82.349	197.434	177	C
Haber	82.689	262.583	34.44	C
Hermite 1	84.82	250.895	241.4	C
Hermite 2	84.686	266.05	60.04	C
Hermite 3	84.932	277.397	35.2	C
Unnamed	83.729	294.149	11.56	C
Florey	85.952	343.106	27.36	C
Gioja	82.766	1.711	40.85	C

Type A PSRs are characterized by having full shadow at a crater floor, resulting in having a high PSR/crater ratio (Figure 1A, D). Due to this full shadow within the crater, the PSR/crater ratio follows a linear relationship, as we expected (Figure 2; R^2 ~0.95). The majority of Type A are located at the more poleward latitudes (Figure 3). In Figure 4, Type A typically have steep crater slopes, from 18 – 28 degrees in both north and south poles.

Type B PSRs are classified as being wall-to-floor contact PSRs, where the PSR is typically at the base of the host crater wall (Figure 1B, E). These Type B have intermediate PSR/crater ratios (Figure 2), though still a fairly linear relationship (R^2 ~ 0.8). Type Bs are the most common type and found across the poles, though the majority of Type B south pole PSRs are more poleward (Figure 3). The slopes for Type B PSRs are from 7 – 22 degrees in the south pole and 10 – 18 degrees in the north pole (Figure 4).

Type C PSRs are categorized as being found primarily at the wall-floor contact similar to Type B (Figures 1C, F), though some only within the crater floor. These have comparably lower PSR/crater area ratios with no clear relationship of the ratio (R^2 < 0.4; Figure 2). From Figure 3, these type PSRs are primarily equatorwards from latitude ~85 degrees in both north and south poles. The slopes are comparably shallower than Type A and B PSRs, with a range of 5 – 13 in the south pole and 4 – 18 degrees in the north pole (Figure 4). We do note some overlap of Type B slopes (on the lower end) to Type C, although the PSR area is more variable for Type B, particularly decreasing in area as slope increases in the south pole (Figure 4b). This may be due to the crater topography influencing the cold area (especially in seasonally varying regions),

therefore influencing the condensation potential of the volatiles. Table 2 summarizes the ranges at which each of these classes are measured.

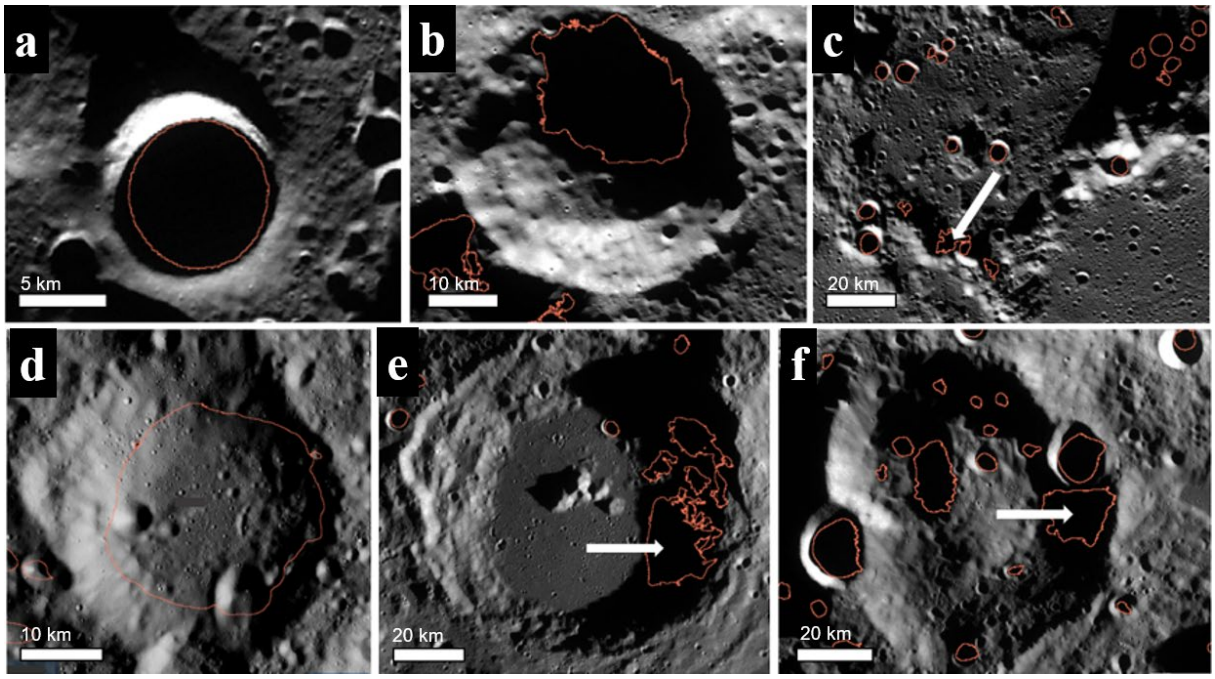

Figure 1: Example PSR types. LROC wide-angle camera base mosaic with PSR boundaries (as orange outlines) as mapped in LROC QuickMap. Examples of PSR types as described in this study from the north (top row) and south (bottom row) lunar poles. a) Erlanger – *Type A*; b) Rozhdestvenskiy U – *Type B*; c) Florey – *Type C*; d) Haworth – *Type A*; e) Amundsen – *Type B*; f) Nobile – *Type C*. White arrows indicate the PSR that was studied within that crater.

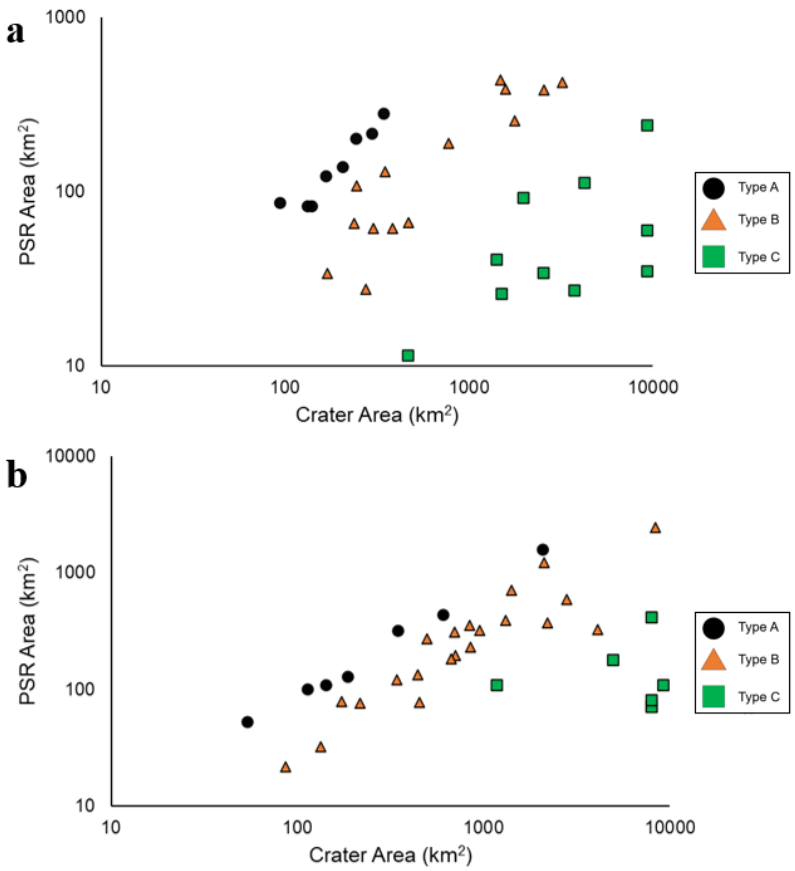

Figure 2: PSR/Crater ratio plots. Area of the PSR compared to their respective host crater area from the North pole (a) and South pole (b).

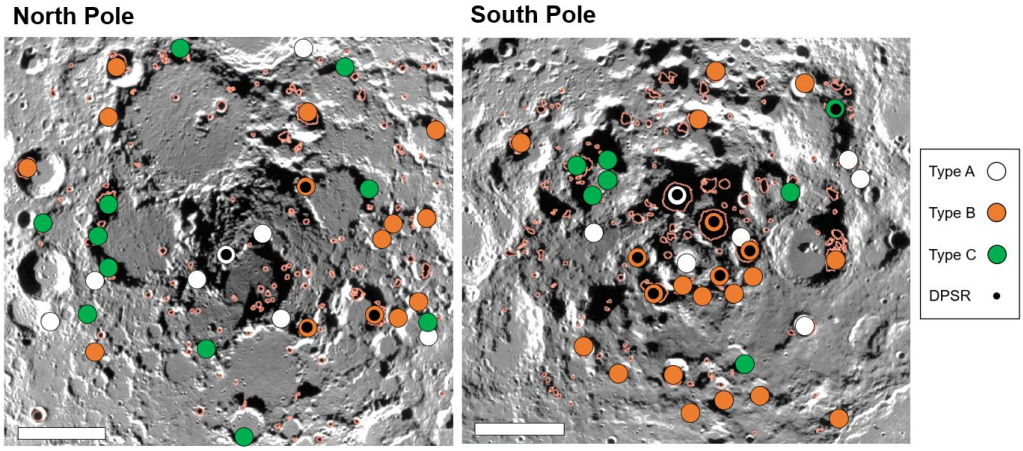

Figure 3: Distribution of PSR types at the lunar north and south poles. Underlying maps are polar LROC mosaics. Black dots within designated-type circles are double-permanently shadowed regions (DPSRs). Scale bar is 100 km.

PSRs are not entirely shielded from illumination. Crater floors and walls are exposed to scattered sunlight and thermal emission, which differs in intensity temporally (O'Brien & Byrne 2022). Topographic depressions within a PSR can not only be shielded from direct sunlight but

also be shielded from these grazing and secondary illumination sources. Double permanently shadowed regions (double PSRs), nested within larger permanently shadowed regions, experience enhanced thermal shielding due to the absence of both direct solar illumination and secondary scattered light. This compounded shading results in lower equilibrium temperatures, making these zones some of the coldest for volatile retention on the lunar surface, noted as black dots in Figure 3. For this study, we utilized the average temperature across the PSR, irrespective of the presence of double PSRs, though we note the inclusion of such colder cold traps may enhance local thermal gradients and influence the overall temperature analysis. Due to their smaller size compared to the larger PSRs and the limitations of current imaging under low illumination, many DPSRs remain unresolved; however, several identified by O'Brien & Byrne (2022) are included in this study, with most located near the lunar south pole.

From our study in the lunar south pole, there were 5 Type B PSRs (De Gerlache, Faustini, Slater, Shoemaker, Sverdrup), 1 Type A (Haworth), and 1 Type C (Nobile) that were observed to have DPSR features. Of note, these PSRs that have double-shadows have > 30 K temperature differences, except for the Type C PSR/DPSR that has a temperature difference of ~8 K. By comparison, the lunar north pole had 3 Type Bs (Fibiger, Nansen F, Bosch), and 1 Type A (Hinshelwood), with these regions being < 20 K temperature differences (Table 2). With current technologies, such as ShadowCam onboard the Korea Aerospace Research Institute (KARI) Korea Pathfinder Lunar Orbiter (KPLO) satellite (Robinson et al. 2023), these may assist in identifying features, such as depressions, within PSRs (Mahanti et al. 2023).

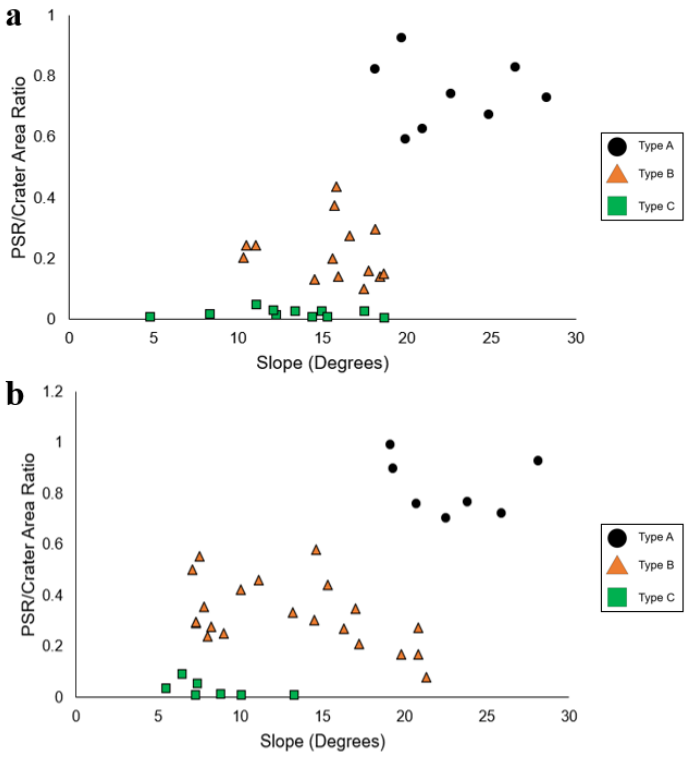

Figure 4: PSR/Crater area ratio versus crater slopes. PSR types shown in the legend. Note that the three types of PSRs from the North (a) and South (b) lunar poles show distinguished

ranges between area ratio to crater slope, namely Type A having relatively higher area ratios and steeper slopes.

Table 2: Summary of PSR parameters measured in this study. This includes the area ratio between the PSR and host crater, slope at which the PSR is observed, and ΔT between maximum summer and winter temperatures from Diviner.

Pole	Type	PSR/Crater Ratio	Slope (°)	ΔT (K)
North	A	0.6–0.98	18-28	10–30
	B	0.09–0.57	10–18	< 20
	C	0.008–0.09	4–18	5–35
South	A	0.6–0.98	18-28	< 60
	B	0.09–0.57	7–22	20–60
	C	0.08–0.09	5–13	5–35

3.2 Thermal Environment

3.2.1 Surface Volatiles and Temperature Differences

The thermal differences at these PSR types could provide some insight to the types of volatiles that may be present. Recent work has used temperature as a constraint on the presence and predicted stability of volatiles at the Moon, namely water, carbon dioxide, and sulfur-bearing compounds (Paige et al. 2010; Williams et al. 2019; Landis et al. 2022). Temperature differences at these PSRs can relate to possible differences in chemical compounds that would deposit within these craters. Mitchell et al. (2018a) and Landis et al. (2022) mapped volatile compositions and defined chemical parameters across the lunar northern and southern poles. Key volatiles come from a variety of origins, which may include solar wind bombardment (McCord et al. 2011), volcanism (Kring et al. 2021), and cometary impact (Mandt et al. 2022). Lunar volcanic activity would help deposit more sulfur to the lunar poles (Needham & Kring 2017), whereas cometary-sourced or other H-bearing impact events would contain more water than sulfur, plus possible additional organic compounds (Eke et al. 2009; Pieters et al. 2009; Zhang & Paige 2009; Bockelée-Morvan 2011).

A catalog of PSR types at the north and south pole can also give us insight to hydrogen (H) abundances. Hydrogen abundances from Lunar Prospector deconvolved maps on LROC QuickMap were compared at the PSR sites. This map allowed us to compare the distribution of H across the created PSR catalog. H abundances (in μg/g) were compared to PSR/Crater ratios of the PSRs (Figure 5). We observe a wide distribution of hydrogen across the different types, from 50 – 250 μg/g, though the majority of north polar PSRs of all types are < 150 μg/g.

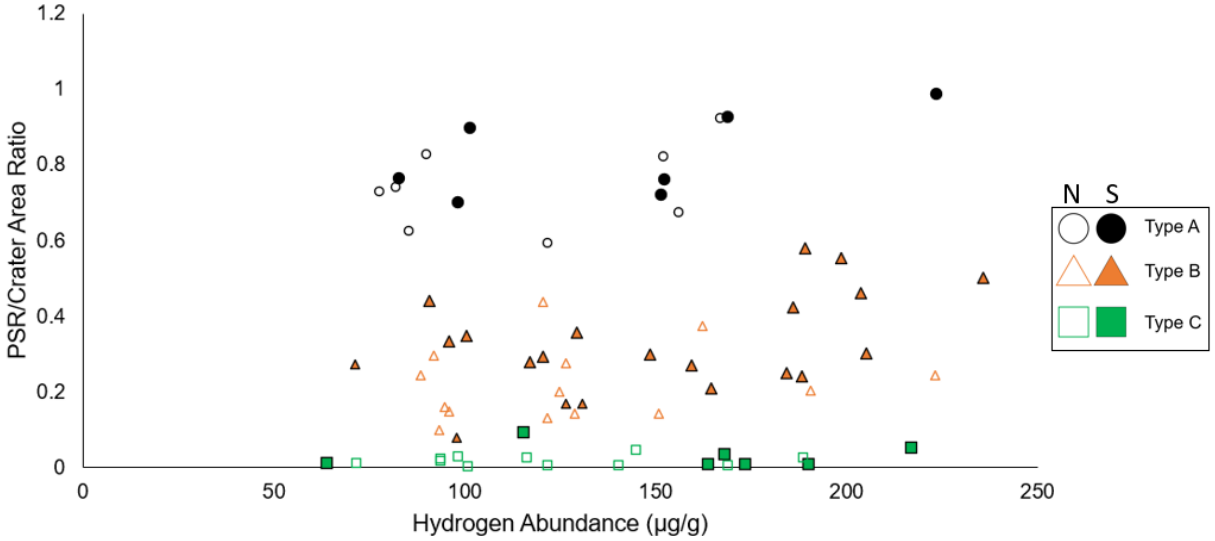

Figure 5: Hydrogen abundances between the north and south pole PSRs in this study. Hydrogen abundances (in µg/g) as measured from Lunar Prospector as compared to PSR/Crater Area ratios. N indicates north; S indicates south.

Water requires ~140 K maximum temperature to freeze, > 175 K for sulfur ices, but < 75 K for other volatile species, such as ammonia, carbon dioxide, or sulfur dioxide (Paige et al. 2010; Mitchell et al. 2018b; Magaña et al. 2023). Maximum summer and maximum winter temperatures within the PSR center allows us to measure the extreme seasonal temperature differences at each of the studied PSR sites (see Figure 6). Observing the thermal differences of maximum summer and winter temperatures (ΔT) using Diviner data at each of the PSR sites can provide us information on the possible chemical interactions and volatile behaviors that may be present, especially if some are seasonally dependent.

Type A has a lower temperature difference in the northern pole than the southern pole, with a difference of 10 – 30 K in the north and up to 60 K in the south. Type Bs are similar to Type As in that the temperature difference is greater in the southern pole than in the north. Type B has a temperature difference between 20 – 60 K in the south pole, and < 20 K difference in the north pole. Type C PSRs are relatively comparable between the north and south pole environments, between 5 – 35 K. It has been mapped by Landis et al. (2022) that potentially more sulfur-related volatile compounds may be thermally stable in the southern pole PSRs, along with Type A in the northern pole. Type Bs may have comparatively more ammonia-type volatiles in the southern pole and less so in the north pole. Volatile organic compounds may also be more prominent in the south pole, along with Type B and C in the north pole. These discrepancies are due to the temperature ranges present at these PSR sites, including the seasonality of temperatures at the PSRs, and the crater geometry in which the PSR is emplaced (e.g., crater depth that may influence the deposition of the volatiles). Type A in the northern pole have a lower temperature difference (< 30 K) than southern pole Type A (> 30 K), which may be conducive to the deposition of more sulfur-type ices that require warmer temperatures (e.g., larger temperature differences). For the Type B and C, the emplacement of the volatiles depends on the thermal stability of which these volatiles may or may not be present. These compounds were modeled based on a decade-worth of Diviner data (see Landis et al. 2022), but the actual

weight percent (let alone confirmation of the existence) of these compounds at these PSR sites are still unknown until more in-situ utilization can be sampled at the PSRs.

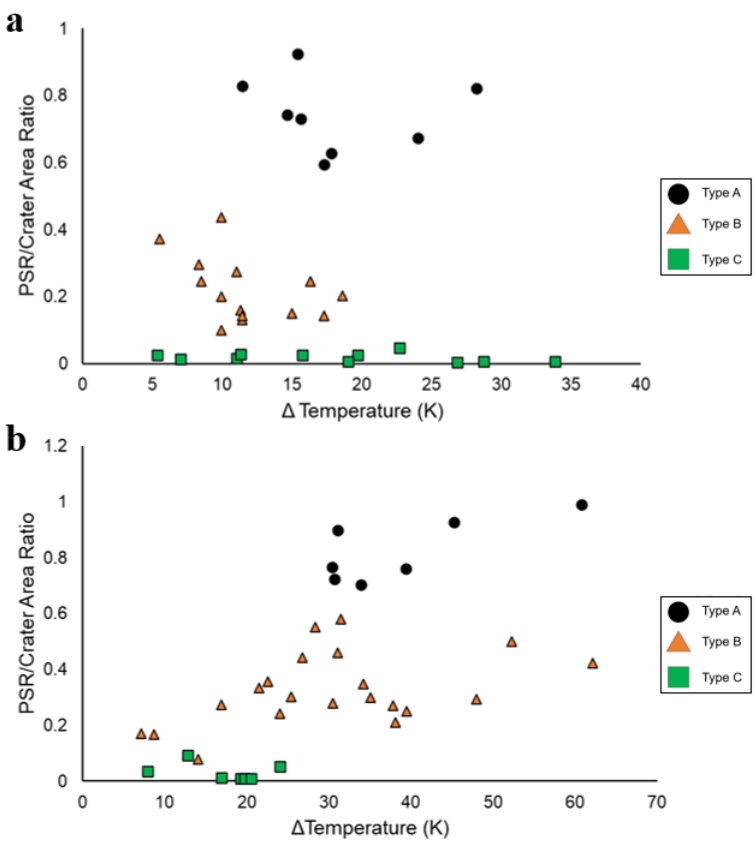

Figure 6: PSR/Crater ratio versus temperature differences. Note the thermal differences of the various PSR types between the north (a) and south (b) poles. Note that Type B in the southern pole have a more diverse thermal difference than Type B in the northern pole.

3.2.2 Heat Flux

Impact craters are the favorable geologic environment for volatile accumulation, depending on the crater size and topography. Unlike Mercury, the Moon has no evidence for Mercury-like nearly pure ice deposits at least 10s of cm thick, with ice concentrations less than a few percent in the top meter of regolith (Ingersoll et al. 1992; Feldman et al. 1998, 2001; Campbell et al. 2006; Colaprete et al. 2010; Sefton-Nash et al. 2019). In an extreme case, the maximum ice deposition of these deposits fills the crater to the shadow line, which may be a cometary deposit from an impact or shower (Ingersoll et al. 1992; Fastook et al. 2019). Treating these ice deposits as cold-based glaciation from deposition conditions, and apart from sublimation lag deposits, this process would be unlikely to leave any significant impact on the crater and terrain. However, Schmidt et al. (2017) has suggested that subsurface ice may play a role in the mobilization of material. Lateral heat conduction from the surrounding surface terrain would contribute to this lubrication mechanism. Ice at depth is relatively warmer than surface ice due to the insulating nature of the ice thickness. Geothermal flux at the base of the ice is key to controlling ice movement and deposition and retention.

Although the accumulation rates and emplacement times of the ice are unknown, it is possible these ice deposits are buried and layered based on stochastic episodic supply of volatiles. The variability of regolith and volatile interactions of PSRs, while still unknown until future in-situ explorations, have been modeled on Mercurian PSRs, which uses the UMISM model (Fastook et al. 2019). Previous 1D thermal models calculating the thermal distribution in PSRs have used scattered solar radiation using the lunar Lambert model (Liu et al. 2021). The UMISM uses similar parameters for lunar surface characteristics from Liu et al. (2021) and references therein. However, this Lambert model does not account for direct solar radiation. We assume a (practically negligible) ablation rate of < -1.0 m/yr for direct sunlit areas of the ice past the PST volume. There is also a current lack of knowledge of the influence of scattered, reflected sunlight that could bounce off topographic features and direct the thermal dynamics inward toward the PSR indirectly (Figure 7). As an end member for the maximum possible extent of ice accumulation in PSRs, this ice deposit is filled to the permanent shadow terminator (PST; Figure 7). Here we discuss the assessment of ice deposition (and retention) behavior at the immediate surface of the PSRs using UMISM. Typically, this process of ice deformation would result in a thinning of ice toward the crater rim and a thickening deposit of ices toward the crater center. Such deposition would tend to drive the frozen volatiles into the PST within the crater, causing immediate ablation at the crater walls and rims (Lawrence 2017; Fastook et al. 2019) and creating definite boundaries of the PSRs within the craters. We observe that direct and reflected sunlight (external) and geothermal heat flux within the regolith (internal, lateral) can potentially influence the accumulation, migration, and intermixing of the volatiles within the PSR. Again, our results show that there are differences between the north and south poles of the Moon for PSRs, including previously discussed thermal differences (Figure 6) and hydrogen abundance (Figure 5). Therefore, the combination of environmental factors at the polar regions complicates how the PSR volatiles are delivered and accumulated, furthering the need for a survey plan of diverse PSRs.

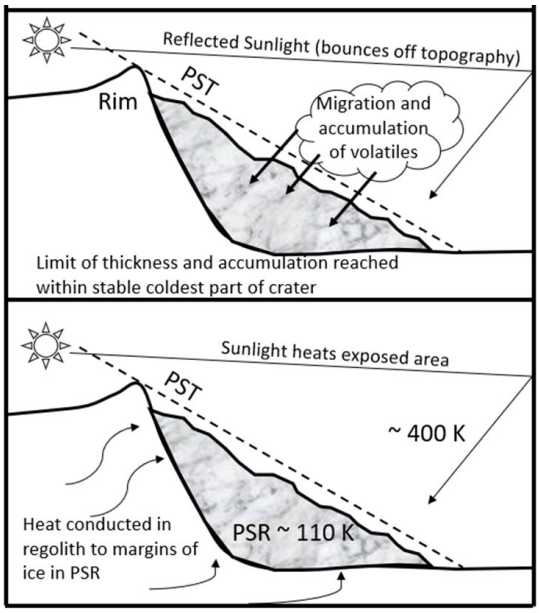

Figure 7: Schematic illustrating ice deposition in permanently shadowed regions at the lunar poles. As volatiles migrate to the coldest regions of the crater, the accumulation of the

deposit would be limited by reflected sunlight, thermal heat retained within the regolith, and the permanent shadow terminator (PST). Figure adapted from Fastook et al. (2019).

Heat flows down the temperature gradient with the flux proportional to the gradient magnitude. In Figure 8, top row, the steepest gradients are observed near the edges of the smallest craters, resulting in the largest contributions of heat to the crater interiors. This is further evident in Figure 9, where the top row shows horizontal flux converging on the crater interior. This source of heat from both sides combines to produce the upwelling of heat observed in the bottom row vertical fluxes. For the smaller craters these sources are inherently closer together, delivering much greater heat to the crater interiors.

Conversely, temperature dependence of thermal conductivity of the regolith can assist in insulating cold surfaces, causing heat flow processes (Woods-Robinson et al. 2019). The heat flux is influenced by the diameter of the crater and is most pronounced near the edges at the surface-temperature discontinuity. Smaller craters therefore have much higher heat fluxes at their centers, decreasing as the crater diameter increases. Heat flow perpendicular to the temperature isotherms focuses the additional flux onto the cold spot base. Accounting for lateral transport of geothermal heat through the bedrock to craters, at least to small craters, suggests that deposits may be limited in retention at the crater walls.

Clearly, lateral transport of the thermal heat from surrounding sunlight of the PSR crater interior must also be taken into consideration, with contributions both vertically and horizontally. This lateral transport into a crater is modelled with a rectangular region, scaled by the depth/diameter ratio of the crater, that extends well into the lunar crust. Potential water ice at PSR ambient temperature below the shadow line defines the temperature at the base of the PSR. Surrounding sunlit terrain is defined to be warm and the temperature gradient at the base of the modelled region is defined by the 10 mW/m^2 heat flux (Fastook et al. 2019). Figure 9 (top row) shows the horizontal component of the heat flux from Figure 8, with considerable heat flowing into the PSR from the surrounding sunlit terrain. For smaller craters these regions of lateral flux are relatively larger and overlap in the middle of the PSR contributing to the heat delivered to the base of the PSR. With larger craters the effect is focused mainly on the crater walls. The bottom row of Figure 9 shows the vertical component of the distorted heat flux field that results from the depression of the isotherms below the cold spot. For smaller craters the entire PSR floor experiences enhanced heating, whereas for larger craters the effect again is focused near the crater walls.

Looking at the smaller crater sizes similar for Type A (Figures 8A,9A), where the crater sizes range from 15 – 21 km, geothermal flux for this crater size tend to have an increase in heat flux directly under the PSR base. As observed in Figure 10A, geothermal fluxes would be so close in proximity between the crater wall and floor at a shallow depth (< 5 km), that the frozen material would mobilize to the center of the crater and stabilize by the lower heat flux at the crater walls.

Type B crater sizes range from 31 – 36 km, where the geothermal heat becomes deeper and have fluxes toward the crater walls (Figure 8B), which are the dominant location of Type B within their host craters. Like Type A, horizontal flux across the crater shows symmetrical distributions (Figure 9B), with lower fluxes at the PSR-dominant side of the crater. Vertical flux is also higher directly under the crater, though the isotherm is much deeper, nearly 3x.

For the larger crater sizes hosting Type C (78 – 89 km diameters), the geothermal flux is disparate across the crater, having lower fluxes at the crater walls, and relatively shallower at the

PSR-side of the crater (Figures 8C, 9C). This may connect with how Type Cs are partial in morphology and are formed at relatively lower slopes than Type A and B.

Understanding these differences in geothermal heat flux shows us the differences in the PSR volatile deposition. These classifications can therefore be used as a source of ISRU based on the thermal characteristics of the PSR environment and identifying the more stable PSRs for future robotic and human explorations. Geothermal properties can also be useful for geotechnical techniques and site planning, especially when handling frozen volatiles at some depth and abundance, which may lead to mining challenges unless thoroughly studied beforehand.

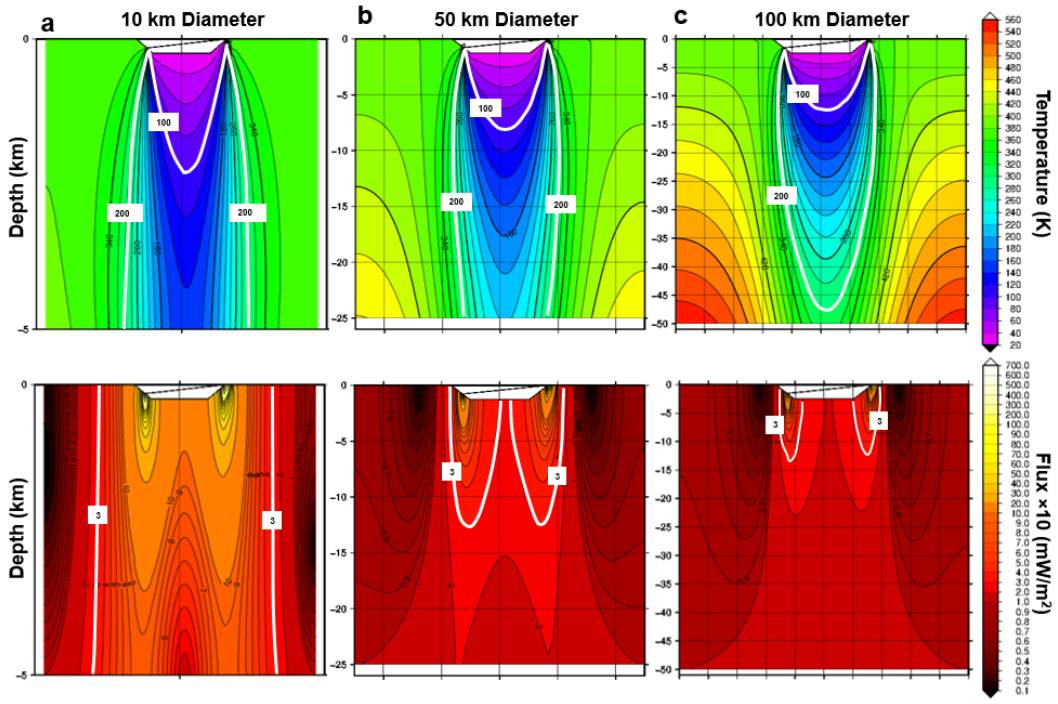

Figure 8: Modeled temperature and heat flux of different sized craters using the UMISM model. Temperature fields (top row) and heat flux fields (bottom row) for 10-km, 50-km, and 100-km diameter cold spots. In all the figures, the black shape at the top indicates the crater depression with some sun angle (slanted line as illustrated within the depression). 100 K and 200 K temperatures are marked. A heat flux of 30 mW/m2 is marked to delineate differences of enhanced heat flux at the edges of the cold spot depression.

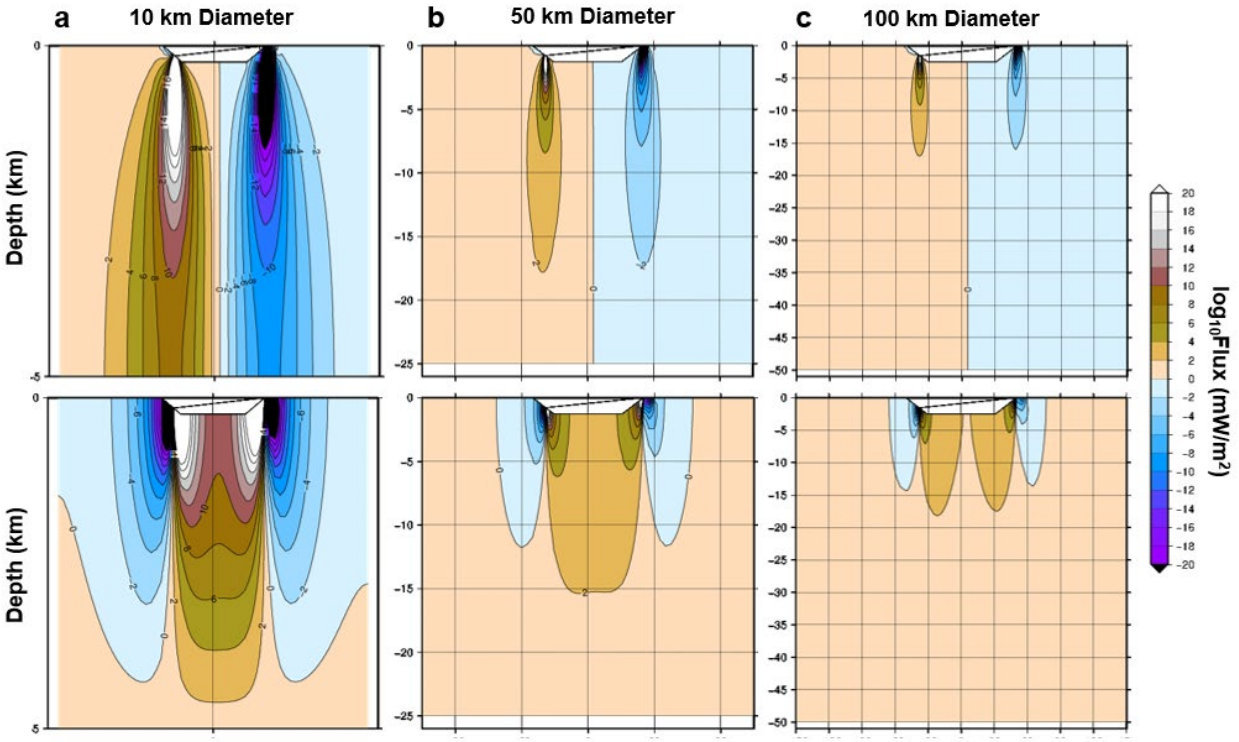

Figure 9: Heat flux parameters of varied crater sizes from the UMISM model. Horizontal flux fields (top row) and vertical flux fields (bottom row) for 10-km, 50-km, and 100-km diameter cold spots. In all the figures, the black shape at the top indicates the crater depression with some sun angle (slanted line as illustrated within the depression).

4. Metrics for Decision Making Systems

4.1 Variable PSR Environments

Other regions of the inner Solar System also have confirmations of water ice (and other volatile species) deposits. At Mercury, the question remains on the differences between processes, timing, and sources (Lawrence 2017). For Ceres, although with the presence of a buried ice table, does have polar crater ice deposits (Hayne and Aharonson 2015). The volatile inventories of the Moon, Mercury, and Ceres are intricately linked to the behavior of their tenuous exospheres and the ongoing interaction with the solar wind. In the absence of substantial atmospheres, these bodies maintain surface-bound exospheres, where volatiles are continuously exchanged between the regolith and the near-surface environment through processes such as thermal desorption, photon-stimulated desorption, micrometeoroid impact vaporization, and ion sputtering (Hurley et al. 2017; Landis et al. 2022). A key contributor to this dynamic system is the implantation of solar wind ions (i.e., hydrogen and helium). These interactions are spatially and temporally variable, governed by factors including local temperature regimes, illumination conditions, and surface composition. From (Hurley et al. 2017 and Hodges, Jr. 2016), nearly up to 50% of incoming solar wind H^+ may be converted to H_2 and up to 76% of solar wind C^+ as CH_4. Hydrogen distribution, while varied between types of PSRs as observed in this study, still shows a variation between the poles, where northern PSRs show lesser abundances of H than

south pole PSRs. Distribution of the ice within these PSR types (whether full coverage at the crater base or partial at the crater wall) implies some difference in compound migration and condensation of the H. DPSRs, especially being more prevalent in the south pole, with pockets of localized thermal sinks may also contribute to the condensation and distribution of H and volatile compounds within the larger PSR environments in which they are found. This further complicates the understanding of hydrogen and carbon cycles at airless bodies, especially at the Moon. Variability and distribution of the hydrogen is one of the prime objectives of Artemis III+ (A3GT 2024).

Also, from this study gave us more questions on the variability of PSRs between the lunar north and south poles. As mentioned earlier, Williams et al. (2019) observed from Diviner that the northern pole has larger increases in winter temperatures than the south pole, implying that migration and abundance of H+ and volatile compounds would vary differently. End-members of PSRs could include the physical environment of which the PSR is found, from the classically deep yet shallower geothermal flux (Type A) versus the morphologically shallower yet thermal disparate environments (Type C). Distinguishing types of PSRs may be needed for mission and traverse planning, especially when Artemis and South Pole – Aiken Basin sample return missions (Moriarty and Pieters 2018; A3GT 2024) want to explore varying mineralogical units, the same could be applied to PSRs in their variability of thermal environments and chemistry.

Regolith characteristics are also a factor in ice stability within PSRs. The role of surface roughness can influence the dispersion (migration) of different volatile compounds, therefore influencing the rate and continuity of volatile accumulation (Rubanenko and Aharonson 2017; Rubanenko 2024). Higher surface roughness could create more shadow areas but may also introduce a level of thermal instability by increasing localized temperature or heat retention in the regolith. At high latitudes, the lunar poles benefit from low solar incidence angles, further decreasing any emitted flux into the shadows (Rubanenko and Aharonson 2017). However, the thermal control of the regolith may still influence the accumulation of different volatile compounds, which may have led to the observation of discrepancies between the northern and southern pole PSR distribution from this study.

PSR distribution is certainly linked to temperature distribution and therefore governed by local topography and subsurface proprieties to some extent. 1D heat diffusion models, with the more recent inclusion of ray tracing and heat conduction models, have improved the understanding of heat transfer mechanisms on the Moon (Aharonson and Schorghofer 2006; Davidsson and Rickman 2014; Hayne and Aharonson 2015). The topography of slopes and craters also govern the amount of shadows and "shadow volume" where ice can potentially accumulate (Rubanenko 2024). Rubanenko (2024) calculated a near-linear relationship between PSR lateral size and shadow volume depth, finding differences in consistent versus sporadic (or episodic) accumulation for PSRs < 10 km (mainly micro cold trap scale). This finding may be useful for Type A PSR behavior, particularly for the stability of volatiles for deeper depressions, but that heating and accumulation (especially if not consistent or continuous in accumulation) may play a larger role in volatile dispersion at these sites. Interestingly, Formisano et al. (2024) modeled sites with high concavity to bear "self-heating", which may explain warming (to a lesser degree) of regions not directly lit by the Sun. PSR sites, with even the morphological differences between Types A, B, and C and northern versus southern poles, each contain specific topographic constraints that need to be further analyzed with the improvement of thermal models. The lateral and vertical heat transport modeling from this study can assist in ice stability region analyses, but small-scale topographic characteristics and shadowing must be enhanced.

Lateral heat transport and topography are vital to further thermal modeling at the lunar poles and for analyzing prospective landing sites, like for ESA's PROSPECT package (Formisano et al. 2024).

Impact craters are the favorable geologic environment for volatile accumulation, depending on the crater size and topography). The lack of an atmosphere on the Moon precludes atmospheric deposition (i.e., net ice accretion), thus resulting in a thermal migration of surface ice accumulation (i.e., migration of compounds from internal or external surface mechanisms such as impacts, cometary impacts, or seasonal flux of compound migration). Heat flows down the temperature gradient with the flux proportional to the gradient magnitude. In Figure 8, top row, the steepest gradients are observed near the edges of the smallest craters, resulting in the largest contributions of heat to the crater interiors. This is further evident in Figure 9, where the top row shows horizontal flux converging on the crater interior. This source of heat from both sides combines to produce the upwelling of heat observed in the bottom row vertical fluxes. For the smaller craters these sources are inherently closer together, delivering much greater heat to the crater interiors. With DPSRs being relatively smaller in size, it is possible that the localized heat may create a thermal sink, possibly attributing to the difference in winter temperature increase differences between the poles (Williams et al. 2019).

Although the accumulation rates and emplacement times of the ice are unknown, it is possible these ice deposits are buried and layered based on stochastic episodic supply of volatiles. As an end member for the maximum possible extent of ice accumulation in PSRs, this ice deposit is filled to the permanent shadow terminator (PST; Figure 7). We observe that reflected sunlight (external) and geothermal heat flux within the regolith (internal) can potentially influence the accumulation, migration, and intermixing of the volatiles within the PSR. Again, our results show that there are differences between the north and south poles of the Moon for PSRs, including thermal differences (Figure 6) and hydrogen abundance (Figure 5). Therefore, the combination of environmental factors at the polar regions complicates how the PSR volatiles are delivered and accumulated, furthering the need for a catalog of diverse PSRs. Spatial awareness of the PSRs can also be useful for site planning purposes. For example, the PST placement and angle at a PSR are also useful for operational planning to assist in equipment and instrument placement needing to be in direct sunlight while also taking measurements of the proximal PSR environment.

4.2 Surveying System for Mission Planning

While most currently planned exploration is reaching the south pole of the Moon, the north pole can provide insight on differences in volatile migration and deposition, which is also a scientific objective of the LRO (Keller et al. 2016). Having a catalog system at PSRs can allow for mission planning and preemptive risks for higher science gain. PSRs, along with landing sites in general, must be scrutinized based on surficial risks, including slopes, illumination conditions, and landing accessibility. However, sampling the PSRs to understand the lunar environment is also a high priority. Thus, having a system can greatly increase our organization and decision-making efficiency in landing site and scientific objective planning. The Artemis III Science Definition Team (SDT) suggests the following factors for site selection: (i) availability of range of crater sizes for traverses and sampling; (ii) comprehensive sampling opportunities; and (iii) proximity and accessibility of permanently shadowed regions. From the recent Lunar Exploration and Analysis Group (LEAG) goals, there is a need for a sampling strategy to account

for the variations in sampling nominal and volatile samples (Goal C) and that having a context of thermally varied areas can be used for traverse planning (and landing site considerations) to assess the nature and abundance of volatiles (transient or thick deposits; Goal D; A3GT 2024).

For example, if a scientific objective wants to sample a specific temperature region at a PSR, but with lower risk regarding illumination and slopes, this will allow PSR Types B and C to be of higher probability of sampling successfully. If a rover or lander can approach an area of higher slopes, but the thermal environment differences must be accounted for due to possible instrumentation limitations, then this limits Type A candidates, with a possible change of plan to a Type C (which has less ΔT changes). The varying types of PSRs also allow for investigation of different geomorphological properties that may be present. That is, the differences in thermal and volatile conditions may influence the surface geomorphology. Having a system assists in such comparative work. Table 3 further discusses how a PSR system fits within the Artemis science priorities.

Table 3: Artemis III Science Definition Team (A3SDT) science objectives and accompanying justification for a PSR survey scheme.

Priority ID	Science Objective	PSR Survey Justification
1a-1	Establish the mechanisms, timing, and extent of volatile depletion in the Moon	Need geological and geochemically diverse samples, including diversity in volatile elements
1f	Regolith processes and weathering	Addition, modification, and alteration of products by micrometeoroid impacts, solar and interstellar charged particles, radiation, spallation, *etc*. may differ at PSR locations
2a	Determine the compositional state (elemental, isotopic, mineralogic) and compositional distribution of the volatile component in lunar polar regions	Pre-determined mapped distribution for planning; ground truthing
2a-1	Identification of surface frost composition	Compositional and thermal diversity at PSR Types A, B, C
2a-2	Identification of surface frost locations in spatial context	Controlling environmental variables regarding volatile deposition/retention
2a-3	Temporal variability of frost	Thermal seasonal variability across different types of PSRs
2a-4	Speciation of surface hydrogen	H-bearing compounds pre-determined by locale; potential diversity in H-bearing compounds, including organics, ammonia
2a-5	Understand surface hydrogen speciation spatial variability	*see 2a-4*
2a-6	Spatial distribution of subsurface hydrogen	PSR Types preemptively determine H-bearing sources and diversity in geothermal fluxes for subsurface parameters
2b	Determine the source(s) for lunar polar volatile deposits	Multiple chemical species from different sources, each deposited differently at the poles and PSR types
2c	Understand the transport, retention, alteration, and loss processes that operate on volatile materials near and at permanently shaded lunar regions	Variations in composition "type" can assess distribution of water/other volatiles and predict ice stability/distribution of volatiles at different PSR types; ground truthing
2c-2	Subsurface temperatures	Understanding the regolith and thermal flux differences at PSR types
2f	Understand the impact of exploration on the lunar volatile record across the surface	Certain types of volatiles should be cautionary to be in proximity during EVA, plus sample/handling activity

4.3 Decision-Making Metric Factors

Within sustainable environmental and site planning efforts, there are several indicators that can be used as a measure of the performance of an operation (i.e., manufacturing or mining unit, a federal or private entity) with respect to a specific external factor (Petrie et al. 2007), such as the environment or human-induced activity. The indicators and importance thereof are subjective and will vary depending on the use of the indicators and on the objectives of the stakeholder or decision-maker.

In the context of sustainable performance on the Moon, categories of indicators can be classified as environmental, social/economic/political, and technical (Petrie et al. 2007). For environmental use at PSRs, these indicators can be measured through remote sensing, robotics, and human activities, relying on data collection and analyses to guide decisions. On the social-economic-political aspect, the mapping of PSRs can lead to collaboration (or conflict) of resource management and sampling. In the technical indicator category, this can span from advancement of technology and sampling techniques at PSRs or the safety and operability of activities at and near PSRs.

These variable indicators can be used for site planning and future optimization models to decide on the extent of surface operations and equipment use. An organized concept of operations (CONOPS) with different activities and interacting with the natural lunar environment, particularly in proximity with PSRs, will be necessary for site planning. Figure 10 shows an example of a decision framework diagram for interacting surface operations and equipment, and what level of interaction could these activities impose on a PSR site nearby.

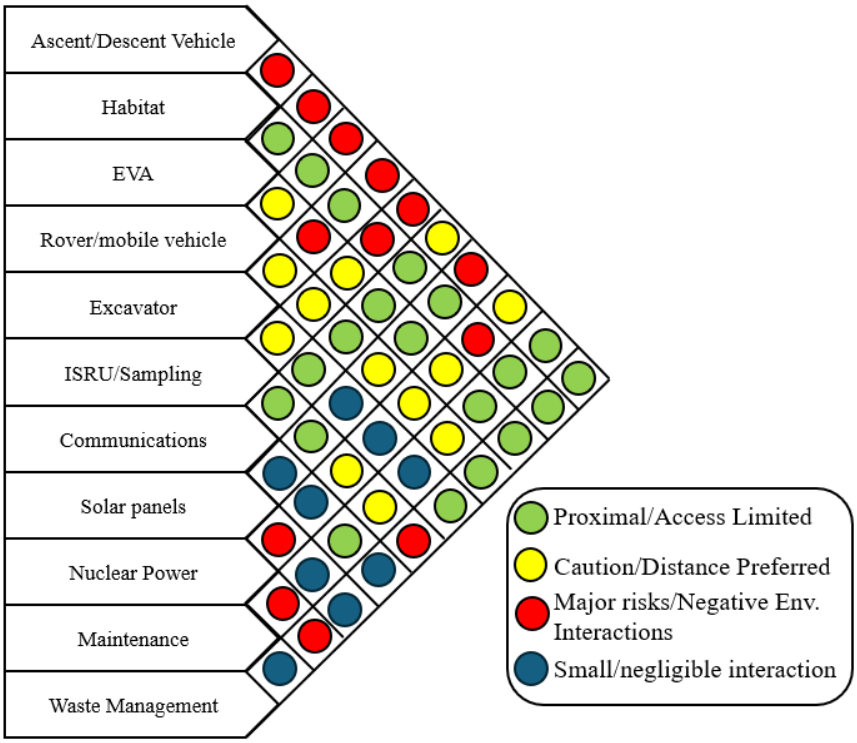

Figure 10: Example decision framework diagram on surface activities within the vicinity of a PSR. This type of diagram can assist in site planning and CONOPS near PSR sites, especially

if some activities can modify the natural environment in a negative way or may need additional monitoring efforts.

There are also several uncertainties regarding science and operations at PSRs. First, the volatile abundance in quality (i.e., purity) and quantity are unknown. The stability and depth of different chemical species, including the molecular migration and accumulation at these regions, are yet known. For operations, the sampling and subsequent monitoring and preservation of lunar polar ices is also unforeseen yet provides an interesting opportunity for robotic and human exploration at these sites before larger and longer-term activities at the poles. The uncertainties from both natural and anthropogenic facets can still be explored in adaptive decision frameworks.

Therefore, the varying types of PSRs can lead to a swath of decision-making endeavors, depending on the entity. Benchmarking or a reporting system of operations at PSRs may be critical to share amongst space actors to define and refine operations and advancing decision making frameworks. Such environmental metrics, such as the illumination and thermal variability at the different PSRs are just a beginning step toward not only understanding natural PSR processes, but also how to best utilize PSRs for resources on the Moon.

4.3.1 Decision Scenarios with a PSR Survey

For a sustainable presence, these measurable indicators can also assist in monitoring the PSRs for degradation of the resources from human and robotic activities. Stated from Petrie et al. (2007), decision making situations are prospective, meaning predictions of the PSR behavior from previously collected data and advancement of models are necessary for decision making. Environmental reporting and monitoring may be key to determine not only the resourcefulness of specific PSRs for a specific operation, but also the observations of environmental influence from human presence (i.e., dust and plume impingement). Here we give a few user scenarios where a PSR environmental survey can be useful for site and operational planning.

Example 1: An exploration team has limited mobility, and instrumentation is required to have some amount of illumination conditions for power constraints. A Type C PSR would be a viable choice for this team as it has been observed that Type C have less slopes < 15° (and some Type B) that pose less mobility risk. Type C PSRs are usually in areas with proximal illuminated areas within the crater, adding safety and increasing Earth-to-Moon communications.

Example 2: If a science objective would be for resource mining and mapping with a variety of chemical species and hydrogen, Type B and Type C in the lunar south pole have more stable cold regions and more H-abundances > 150 ug/g. However, Type A may have more sulfur-rich volatiles due to higher temperature ranges, but may pose a risk to equipment enduring such extreme thermal differences. Type A are also of greater risk due to the slopes. On the other hand, an exploration for testing mining equipment and operations near a PSR may find a Type C more helpful and sparser in frozen volatile abundance, if not for safety reasons.

Example 3: An excavation team may need to survey the site from geotechnical techniques before major operations. Type As are typically smaller craters, therefore bearing more localized geothermal heat at the center of the crater. Type Cs, while larger craters, also have

more dispersion of geothermal heat flux at the crater walls compared to the center. This localized difference in geothermal heat may influence the geotechnical properties of the regolith and volatile retention of the regolith. Understanding the geotechnical properties can also be useful for 3D printing operations but will require ground truthing of regolith properties at varying PSR sites.

Surveying PSRs for decision-making and operational constraints can be useful for not just the scientific aspect of how PSRs are distributed across the lunar poles, but also knowing the types of PSRs can also assist in conservation decisions if preservation of lunar volatile ices at certain regions are warranted.

5 Conclusions

Hence, understanding the thermal environment and morphology of the craters that house these PSRs, including the subsurface thermal flux of the impacts, can be insightful to organize a PSR decision-making framework. Utilizing various remote sensing techniques and measurements to form a PSR survey into the context of environmental factors, surface chemistry, and potential loss processes are all critical information needed not only for numerical modeling and sample analysis, but also science and mission planning objectives.

We find that the PSRs studied here offer variations of thermal and chemical properties between lunar north and south poles. Based on our analysis of the factors important in PSR surveying, we note that:

1. The emplacement of certain volatile chemical species relies on these permanently shadowed regions, and thus depends on the environmental conditions, such as regolith geothermal flux and illumination conditions, leading to variations in PSR creation and volatile stability into three distinct types.
2. Understanding the spatial distribution of PSRs is essential for site planning, though significant uncertainties in volatile abundance, thermal behavior, and other natural variables highlight the need for further ground-truth exploration while presenting both challenges and research opportunities.
3. Environmental modeling from remote sensing data in addition to this PSR survey can be optimized for decision-making frameworks for site planning, especially for a variety of space actors, CLPS, and Artemis.
4. Varying types of PSRs can lead to variations in exploration (and preservation) options and CONOPS of surface activities, depending on scientific and technical objectives, risk, and PSR stability in proximity to the operations.

Acknowledgments

This research was supported by an appointment to the NASA Postdoctoral Program at the NASA Goddard Space Flight Center, administered by Oak Ridge Associated Universities under contract with NASA. The material is also supported by cooperative agreement with NASA under award number 80GSFC24M0006. Special thanks to the LRO Diviner team and the NASA Exploration Science Forum & European Lunar Symposium workshop for support and feedback. We also thank two anonymous reviewers and the editor for comments and edits.

References

Aharonson, O., & Schorghofer, N. (2006). Subsurface ice on Mars with rough topography. *Journal of Geophysical Research: Planets*, *111*(E11). https://doi.org/10.1029/2005JE002636

[dataset] Ahrens, C. (2024). Lunar PSR catalog: Area, Length, Slope, H/L ratio. Zenodo. https://doi.org/10.5281/zenodo.14187934

Arnold, J. R. (1979). Ice in the lunar polar regions. *Journal of Geophysical Research: Solid Earth*, 84(B10), 5659-5668. https://doi.org/10.1029/JB084iB10p05659

Artemis III Geology Team (A3GT) (2024). Artemis III Geology Team LEAG Update 10/28/2024. Lunar Exploration Analysis Group Fall Meeting, October 2024. [Powerpoint]. https://www.lpi.usra.edu/leag/documents/A3GT-LEAG_20241028.pdf

Bickel, V. T., Moseley, B., Hauber, E., et al. (2022). Cryogeomorphic characterization of shadowed regions in the Artemis exploration zone. *Geophysical Research Letters*, 49(16), e2022GL099530. https://doi.org/10.1029/2022GL099530

Bockelée-Morvan, D. (2011). An overview of comet composition. *Proceedings of the International Astronomical Union*, *7*(S280), 261-274. https://doi.org/10.1017/S1743921311025038

Brown, H. M., Boyd, A. K., Denevi, B. W., et al. (2022). Resource potential of lunar permanently shadowed regions. *Icarus*, 377, 114874. https://doi.org/10.1016/j.icarus.2021.114874

Bussey, D. B. J., Spudis, P. D., Robinson, M. S. (1999). Illumination conditions at the lunar south pole. *Geophysical Research Letters*, 26(9),1187–119. https://doi.org/10.1029/1999GL900213

Bussey DB, McGovern JA, Spudis PD, et al. (2010). Illumination conditions of the south pole of the Moon derived using Kaguya topography. *Icarus*, 208(2),558-64. https://doi.org/10.1016/j.icarus.2010.03.028

Campbell, D. B., Campbell, B. A., Carter, L. M., et al. (2006). No evidence for thick deposits of ice at the lunar south pole. *Nature*, 443(7113), 835-837. https://doi.org/10.1038/nature05167

Chen, K., Harris, A., Draskovic, J., et al. (2009). Granular fragility under thermal cycles. *Granular Matter*, 11, 237-242. https://doi.org/10.1007/s10035-009-0141-7

Colaprete, A., Schultz, P., Heldmann, J., et al. (2010). Detection of water in the LCROSS ejecta plume. *Science*, 330(6003), 463-468. https://doi.org/10.1126/science.1186986

Collins, G. S., Melosh, H. J. (2003). Acoustic fluidization and the extraordinary mobility of sturzstroms. *Journal of Geophysical Research: Solid Earth*, 108(B10). https://doi.org/10.1029/2003JB002465

Davidsson, B. J., & Rickman, H. (2014). Surface roughness and three-dimensional heat conduction in thermophysical models. *Icarus*, *243*, 58-77. https://doi.org/10.1016/j.icarus.2014.08.039

de Blasio, F. V. (2011). *Introduction to the physics of landslides: lecture notes on the dynamics of mass wasting*. Springer Science & Business Media, Springer Netherlands.

Duarte, K. D., Schmidt, B. E., Chilton, H. T., et al. (2019). Landslides on Ceres: Diversity and geologic context. *Journal of Geophysical Research: Planets*, 124(12), 3329-3343. https://doi.org/10.1029/2018JE005673

Durga Prasad, K., Rai, V. K., & Murty, S. V. S. (2022). A comprehensive 3D thermophysical model of the lunar surface. Earth and Space Science, 9(12), e2021EA001968. https://doi.org/10.1029/2021EA001968

Eke, V. R., Teodoro, L. F. A., Elphic, R. C. (2009). The spatial distribution of polar hydrogen deposits on the Moon. *Icarus*, 200(1), 12-18. https://doi.org/10.1016/j.icarus.2008.10.013

Fastook, J. L., & Head, J. W. (2015). Glaciation in the Late Noachian Icy Highlands: Ice accumulation, distribution, flow rates, basal melting, and top-down melting rates and patterns. *Planetary and Space Science*, 106, 82-98. https://doi.org/10.1016/j.pss.2014.11.028

Fastook, J. L., Head, J. W., Marchant, D. R., et al. (2012). Early Mars climate near the Noachian–Hesperian boundary: Independent evidence for cold conditions from basal melting of the south polar ice sheet (Dorsa Argentea Formation) and implications for valley network formation. *Icarus*, 219(1), 25-40. https://doi.org/10.1016/j.icarus.2012.02.013

Fastook, J. L., Head, J. W., Deutsch, A. N. (2019). Glaciation on Mercury: Accumulation and flow of ice in permanently shadowed circum-polar crater interiors. *Icarus*, 317, 81-93. https://doi.org/10.1016/j.icarus.2018.07.004

Feldman, W. C., Maurice, S., Binder, A. B., et al. (1998). Fluxes of fast and epithermal neutrons from Lunar Prospector: Evidence for water ice at the lunar poles. *Science*, 281(5382), 1496-1500. https://doi.org/10.1126/science.281.5382.1496

Feldman, W. C., Maurice, S., Lawrence, D. J., et al. (2001). Evidence for water ice near the lunar poles. *Journal of Geophysical Research: Planets*, 106(E10), 23231-23251. https://doi.org/10.1029/2000JE001444

Feng, J., & Siegler, M. A. (2021). Reconciling the infrared and microwave observations of the lunar south pole: A study on subsurface temperature and regolith density. *Journal of Geophysical Research: Planets*, 126(9), e2020JE006623. https://doi.org/10.1029/2020JE006623

Fernandes, N. F., & Dietrich, W. E. (1997). Hillslope evolution by diffusive processes: The timescale for equilibrium adjustments. *Water Resources Research*, 33(6), 1307-1318. https://doi.org/10.1029/97WR00534

Fisher, E. A., Lucey, P. G., Lemelin, M., et al. (2017). Evidence for surface water ice in the lunar polar regions using reflectance measurements from the Lunar Orbiter Laser Altimeter and temperature measurements from the Diviner Lunar Radiometer Experiment. *Icarus*, 292, 74-85. https://doi.org/10.1016/j.icarus.2017.03.023

Formisano, M., De Sanctis, M. C., Boazman, S., Frigeri, A., Heather, D., et al. (2024). Thermal modeling of the lunar South Pole: Application to the PROSPECT landing site. *Planetary and Space Science*, *251*, 105969. https://doi.org/10.1016/j.pss.2024.105969

Gertsch, L., Gustafson, R., & Gertsch, R. (2006). Effect of water ice content on excavatability of lunar regolith. In: *AIP conference proceedings* (Vol. 813, No. 1, pp. 1093-1100). American Institute of Physics. https://doi.org/10.1063/1.2169290

Gläser, P., Scholten, F., De Rosa, D., et al. (2014). Illumination conditions at the lunar south pole using high resolution Digital Terrain Models from LOLA. *Icarus*, 243, 78-90. https://doi.org/10.1016/j.icarus.2014.08.013

Gläser, P., Oberst, J., Neumann, G. A., et al. (2018). Illumination conditions at the lunar poles: Implications for future exploration. *Planetary and Space Science*, 162, 170-178. https://doi.org/10.1016/j.pss.2017.07.006

Hayne, P. O., & Aharonson, O. (2015). Thermal stability of ice on Ceres with rough topography. *Journal of Geophysical Research: Planets*, *120*(9), 1567-1584.

Hayne, P. O., Aharonson, O., & Schörghofer, N. (2021). Micro cold traps on the Moon. *Nature Astronomy*, 5(2), 169-175. https://doi.org/10.1038/s41550-020-1198-9

Hayne, P. O., Hendrix, A., Sefton-Nash, E., et al. (2015). Evidence for exposed water ice in the Moon's south polar regions from Lunar Reconnaissance Orbiter ultraviolet albedo and temperature measurements. *Icarus*, 255, 58-69. https://doi.org/10.1016/j.icarus.2015.03.032

Hayne, P. O., Bandfield, J. L., Siegler, M. A., et al. (2017). Global regolith thermophysical properties of the Moon from the Diviner Lunar Radiometer Experiment. *Journal of Geophysical Research: Planets*, 122(12), 2371-2400. https://doi.org/10.1002/2017JE005387

Hibbitts, C. A., Grieves, G. A., Poston, M. J., et al. (2011). Thermal stability of water and hydroxyl on the surface of the Moon from temperature-programmed desorption measurements of lunar analog materials. *Icarus*, 213(1), 64-72. https://doi.org/10.1016/j.icarus.2011.02.015

Hodges Jr, R. R. (2016). Methane in the lunar exosphere: Implications for solar wind carbon escape. *Geophysical Research Letters*, *43*(13), 6742-6748.

Hodges Jr, R. R. (2018). Semiannual oscillation of the lunar exosphere: Implications for water and polar ice. *Geophysical Research Letters*, 45(15), 7409-7416. https://doi.org/10.1029/2018GL077745

Hooke, R. L., & Fastook, J. (2007). Thermal conditions at the bed of the Laurentide ice sheet in Maine during deglaciation: implications for esker formation. *Journal of Glaciology*, 53(183), 646-658. doi:10.3189/002214307784409243

Horai, K. I., & Fujii, N. (1972). Thermophysical properties of lunar material returned by Apollo missions. The moon, 4(3), 447-475. https://doi.org/10.1007/BF00562011

Hurley, D. M., Cook, J. C., Retherford, K. D., Greathouse, T., Gladstone, G. R., Mandt, K., ... & Stern, S. A. (2017). Contributions of solar wind and micrometeoroids to molecular hydrogen in the lunar exosphere. *Icarus*, *283*, 31-37.

Hurley, D. M., Siegler, M. A., Cahill, J. T., et al. (2023). Surface volatiles on the Moon. Reviews in Mineralogy and Geochemistry, 89(1), 787-827. https://doi.org/10.2138/rmg.2023.89.18

Ingersoll, A. P., Svitek, T., Murray, B. C. (1992). Stability of polar frosts in spherical bowl-shaped craters on the Moon, Mercury, and Mars. *Icarus*, 100(1), 40-47. https://doi.org/10.1016/0019-1035(92)90016-Z

Johnson, B. C., & Sori, M. M. (2020). Landslide morphology and mobility on ceres controlled by topography. *Journal of Geophysical Research: Planets*, 125(12), e2020JE006640. https://doi.org/10.1029/2020JE006640

Keller, J. W., Petro, N. E., & Vondrak, R. R. (2016). The Lunar Reconnaissance Orbiter Mission–Six years of science and exploration at the Moon. *Icarus*, *273*, 2-24.

Kloos, J. L., Moores, J. E., Sangha, J., et al. (2019). The temporal and geographic extent of seasonal cold trapping on the Moon. *Journal of Geophysical Research: Planets*, 124(7), 1935-1944. https://doi.org/10.1029/2019JE006003

Kring, D. A., Kramer, G. Y., Bussey, D. B. J., et al. (2021). Prominent volcanic source of volatiles in the south polar region of the Moon. *Advances in Space Research*, 68(11), 4691-4701. https://doi.org/10.1016/j.asr.2021.09.008

Landis, M. E., Hayne, P. O., Williams, J. P., et al. (2022). Spatial distribution and thermal diversity of surface volatile cold traps at the lunar poles. The Planetary Science Journal, 3(2), 39. 10.3847/PSJ/ac4585

Lawrence, D. J. (2017). A tale of two poles: Toward understanding the presence, distribution, and origin of volatiles at the polar regions of the Moon and Mercury. *Journal of Geophysical Research: Planets*, 122(1), 21-52. https://doi.org/10.1002/2016JE005167

Legros, F. (2002). The mobility of long-runout landslides. *Engineering geology*, 63(3-4), 301-331. https://doi.org/10.1016/S0013-7952(01)00090-4

Li, S., Lucey, P. G., Milliken, R. E., et al. (2018). Direct evidence of surface exposed water ice in the lunar polar regions. *Proceedings of the National Academy of Sciences*, 115(36), 8907-8912. https://doi.org/10.1073/pnas.1802345115

Liu, N., & Jin, Y. Q. (2020). Simulation and data analysis of the temperature distribution and variation in the permanent shaded region of the Moon. IEEE Transactions on Geoscience and Remote Sensing, 59(4), 2962-2972. doi: 10.1109/TGRS.2020.3009117

Lucchitta, B. K. (1987). Valles Marineris, Mars: Wet debris flows and ground ice. *Icarus*, 72(2), 411-429. https://doi.org/10.1016/0019-1035(87)90183-7

Magaña, L. O., Retherford, K. D., Byron, B. D., et al. (2023). LRO-LAMP Lunar South Pole Cold Traps: Assessment of H2O and Potential CO2 and NH3 Reserves. *Journal of Geophysical Research: Planets*, e2023JE007863. https://doi.org/10.1029/2023JE007863

Mahanti, P., Robinson, M. S., Wagner, R., et al. (2023, July). First look, first results-comparing secondary illumination at lunar permanently shadowed regions from the first shadowcam image and topography based simulation. *IGARSS 2023-2023 IEEE International Geoscience and Remote Sensing Symposium* (pp. 4162-4165). IEEE. 10.1109/IGARSS52108.2023.10282497.

Mandt, K. E., Mousis, O., Hurley, D., et al. (2022). Exogenic origin for the volatiles sampled by the Lunar CRater Observation and Sensing Satellite impact. *Nature Communications*, 13(1), 642. https://doi.org/10.1038/s41467-022-28289-6

Margot, J. L., Campbell, D. B., Jurgens, R. F., et al. (1999). Topography of the lunar poles from radar interferometry: A survey of cold trap locations. *Science*, 284(5420), 1658-1660. https://doi.org/10.1126/science.284.5420.1658

Mazarico, E., Neumann, G. A., Smith, D. E., et al. (2011). Illumination conditions of the lunar polar regions using LOLA topography. *Icarus*, 211(2), 1066-1081. https://doi.org/10.1016/j.icarus.2010.10.030

McCord, T. B., Taylor, L. A., Combe, J. P., et al. (2011). Sources and physical processes responsible for OH/H2O in the lunar soil as revealed by the Moon Mineralogy Mapper (M3). *Journal of Geophysical Research: Planets*, 116(E6). https://doi.org/10.1029/2010JE003711

McGovern, J. A., Bussey, D. B., Greenhagen, B. T., et al. (2013). Mapping and characterization of non-polar permanent shadows on the lunar surface. *Icarus*, 223(1), 566-581. https://doi.org/10.1016/j.icarus.2012.10.018

Mitchell, J., Lawrence, S., Robinson, M., et al. (2018a). Using complementary remote sensing techniques to assess the presence of volatiles at the lunar north pole. *Planetary and Space Science*, 162, 133-147. https://doi.org/10.1016/j.pss.2017.07.015

Mitchell, J. L., Gruener, J. E., Lawrence, S. J., et al. (2018b). Temperature Constraints on the Storage and Curation of Volatile-Rich Samples from the Lunar Poles. In: *Lunar Polar Volatiles*, USRA, Baltimore, MD Aug. 7 – 8, 2018. No. JSC-E-DAA-TN57277.

Mitchell, J. L., Zeigler, R. A., McCubbin, F. M., Needham, D. H., Amick, C. L., Lewis, E. K., ... & Lawrence, S. J. (2020, March). Artemis Curation: Preparing for Sample Return from the Lunar South Pole. In *Lunar and Planetary Science Conference* (No. JSC-E-DAA-TN77635).

Moon, S., Paige, D. A., Siegler, M. A., et al. (2021). Geomorphic evidence for the presence of ice deposits in the permanently shadowed regions of Scott-E crater on the moon. *Geophysical Research Letters*, 48(2), e2020GL090780. https://doi.org/10.1029/2020GL090780

Moriarty III, D. P., & Pieters, C. M. (2018). The character of South Pole-Aitken Basin: Patterns of surface and subsurface composition. *Journal of Geophysical Research: Planets*, *123*(3), 729-747.

Needham, D. H., & Kring, D. A. (2017). Lunar volcanism produced a transient atmosphere around the ancient Moon. *Earth and Planetary Science Letters*, 478, 175-178. https://doi.org/10.1016/j.epsl.2017.09.002

O'Brien, P., & Byrne, S. (2022). Double shadows at the lunar poles. *The Planetary Science Journal*, 3(11), 258. 10.3847/PSJ/ac9e5b

Paige, D. A., Siegler, M. A., Zhang, J. A., et al. (2010). Diviner lunar radiometer observations of cold traps in the Moon's south polar region. *Science, 330(6003),* 479-482. https://doi.org/10.1126/science.1187726

Parekh, R., Otto, K. A., Jaumann, R., et al. (2021). Influence of volatiles on mass wasting processes on Vesta and Ceres. *Journal of Geophysical Research: Planets*, 126(3), e2020JE006573. https://doi.org/10.1029/2020JE006573

Pieters, C. M., Goswami, J. N., Clark, R. N., et al. (2009). Character and spatial distribution of OH/H2O on the surface of the Moon seen by M3 on Chandrayaan-1. *Science*, 326(5952), 568-572. https://doi.org/10.1126/science.1178658

Prem, P., Goldstein, D. B., Varghese, P. L., et al. (2018). The influence of surface roughness on volatile transport on the Moon. *Icarus*, 299, 31-45. https://doi.org/10.1016/j.icarus.2017.07.010

Robinson, M. S., Brylow, S. M., Tschimmel, M. E., et al. (2010). Lunar reconnaissance orbiter camera (LROC) instrument overview. *Space science reviews*, 150, 81-124. https://doi.org/10.1007/s11214-010-9634-2

Robinson, M. S., Brylow, S. M., Caplinger, M. A., et al. (2023). ShadowCam instrument and investigation overview. *Journal of Astronomy and Space Sciences*, 40(4), 149-171. https://doi.org/10.5140/JASS.2023.40.4.149

Rubanenko, L. (2024). The ephemeral state of ice in micro cold traps on the Moon. *Icarus*, *421*, 116199. https://doi.org/10.1016/j.icarus.2024.116199

Rubanenko, L., & Aharonson, O. (2017). Stability of ice on the Moon with rough topography. *Icarus*, 296, 99-109. https://doi.org/10.1016/j.icarus.2017.05.028

Sanin, A. B., Mitrofanov, I. G., Litvak, M. L., Malakhov, A., Boynton, W. V., Chin, G., ... & Zuber, M. T. (2012). Testing lunar permanently shadowed regions for water ice: LEND results from LRO. Journal of Geophysical Research: Planets, 117(E12). https://doi.org/10.1029/2011JE003971

Schmidt, B. E., Hughson, K. H., Chilton, H. T., et al. (2017). Geomorphological evidence for ground ice on dwarf planet Ceres. *Nature Geoscience*, 10(5), 338-343. https://doi.org/10.1038/ngeo2936

Schörghofer, N., & Rufu, R. (2023). Past extent of lunar permanently shadowed areas. *Science Advances*, 9(37), eadh4302. https://doi.org/10.1126/sciadv.adh4302

Schörghofer, N., & Taylor, G. J. (2007). Subsurface migration of H2O at lunar cold traps. *Journal of Geophysical Research: Planets*, 112(E2). https://doi.org/10.1029/2006JE002779

Schörghofer, N., Lucey, P., Williams, J. P. (2017). Theoretical time variability of mobile water on the Moon and its geographic pattern. *Icarus*, 298, 111-116. https://doi.org/10.1016/j.icarus.2017.01.029

Schörghofer, N., Benna, M., Berezhnoy, A. A., et al. (2021a). Water group exospheres and surface interactions on the Moon, Mercury, and Ceres. *Space Science Reviews*, 217(6), 74. https://doi.org/10.1007/s11214-021-00846-3

Schörghofer, N., Williams, J. P., Martinez-Camacho, J., et al. (2021b). Carbon dioxide cold traps on the moon. *Geophysical Research Letters*, 48(20), e2021GL095533. https://doi.org/10.1029/2021GL095533

Sefton-Nash, E., Williams, J. P., Greenhagen, B. T., et al. (2019). Evidence for ultra-cold traps and surface water ice in the lunar south polar crater Amundsen. *Icarus*, 332, 1-13. https://doi.org/10.1016/j.icarus.2019.06.002

Siegler, M. A., Bills, B. G., Paige, D. A. (2011). Effects of orbital evolution on lunar ice stability. *Journal of Geophysical Research: Planets*, 116(E3). https://doi.org/10.1029/2010JE003652

Siegler, M. A., & Smrekar, S. E. (2014). Lunar heat flow: Regional prospective of the Apollo landing sites. *Journal of Geophysical Research: Planets*, 119(1), 47-63. https://doi.org/10.1002/2013JE004453

Singer, K. N., McKinnon, W. B., Schenk, P. M., et al. (2012). Massive ice avalanches on Iapetus mobilized by friction reduction during flash heating. *Nature Geoscience*, 5(8), 574-578. https://doi.org/10.1038/ngeo1526

Song, H., Zhang, J., Ni, D., et al. (2021). Investigation on in-situ water ice recovery considering energy efficiency at the lunar south pole. *Applied Energy*, 298, 117136. https://doi.org/10.1016/j.apenergy.2021.117136

Thomson, B. J., Fassett, C. I., Bhiravarasu, S. S., et al. (2023). Characterization of Lunar Ice Stability Region (ISR) Host Craters: Size Distribution and Age Constraints. *54th Lunar and Planetary Science Conference*, held 13-17 March, 2023 at The Woodlands, Texas and virtually. *LPI Contributions*, 2806, 2560.

Tooley, C. R., Houghton, M. B., Saylor, R. S., et al. (2010). Lunar Reconnaissance Orbiter mission and spacecraft design. *Space Science Reviews*, 150, 23-62. https://doi.org/10.1007/s11214-009-9624-4

Wilcoski, A. X., Hayne, P. O., Elder, C. M. (2023). Thermal environments and volatile stability within lunar pits and caves. *Journal of Geophysical Research: Planets*, e2023JE007758. https://doi.org/10.1029/2023JE007758

Williams, J. P., Greenhagen, B. T., Paige, D. A., et al. (2019). Seasonal polar temperatures on the Moon. *Journal of Geophysical Research: Planets*, 124(10), 2505-2521. https://doi.org/10.1029/2019JE006028

Wilson, J. T., Lawrence, D. J., Peplowski, P. N., Cahill, J. T., Eke, V. R., Massey, R. J., & Teodoro, L. F. (2018). Image reconstruction techniques in neutron and gamma ray spectroscopy: Improving Lunar Prospector data. *Journal of Geophysical Research: Planets*, *123*(7), 1804-1822.

Woods-Robinson, R., Siegler, M. A., & Paige, D. A. (2019). A model for the thermophysical properties of lunar regolith at low temperatures. *Journal of Geophysical Research: Planets*, 124(7), 1989-2011. https://doi.org/10.1029/2019JE005955

936 Zhang, J. A., & Paige, D. A. (2009). Cold-trapped organic compounds at the poles of the
937 Moon and Mercury: Implications for origins. *Geophysical Research Letters*, 36(16).
938 https://doi.org/10.1029/2009GL038614